Computer Modeling in Engineering & Sciences

Tech Science Press

DOI: 10.32604/cmes.2023.031399

ARTICLE

Numerical Study of the Biomechanical Behavior of a 3D Printed Polymer Esophageal Stent in the Esophagus by BP Neural Network Algorithm

Guilin Wu[1,2], Shenghua Huang[1], Tingting Liu[3], Zhuoni Yang[3], Yuesong Wu[2], Guihong Wei[1], Peng Yu[1,*], Qilin Zhang[4], Jun Feng[4] and Bo Zeng[5,*]

[1]College of Civil Engineering and Architecture, Key Laboratory of Disaster Prevention and Structural Safety of Ministry of Education, Guangxi Key Laboratory of Disaster Prevention and Structural Safety, Scientific Research Center of Engineering Mechanics, Guangxi University, Nanning, 530004, China

[2]Anaesthesiology Department of the 923th, The 923th Hospital of PLA Joint Logistic Support Force, Nanning, 530021, China

[3]Biomedical Materials Engineering Research Center, Tsinghua Innovation Center in Dongguan, Dongguan, 523808, China

[4]Research Centre, Guangxi Nanning Ruifeng Medical Devices Co., Ltd., Nanning, 530000, China

[5]Department of Thoracic Surgery, The First Affiliated Hospital, Sun Yat-sen University, Guangzhou, 510080, China

*Corresponding Authors: Peng Yu. Email: py@gxu.edu.cn; Bo Zeng. Email: zengb7@mail.sysu.edu.cn

Received: 12 June 2023 Accepted: 17 July 2023 Published: 15 December 2023

ABSTRACT

Esophageal disease is a common disorder of the digestive system that can severely affect the quality of life and prognosis of patients. Esophageal stenting is an effective treatment that has been widely used in clinical practice. However, esophageal stents of different types and parameters have varying adaptability and effectiveness for patients, and they need to be individually selected according to the patient's specific situation. The purpose of this study was to provide a reference for clinical doctors to choose suitable esophageal stents. We used 3D printing technology to fabricate esophageal stents with different ratios of thermoplastic polyurethane (TPU)/(Poly-ε-caprolactone) PCL polymer, and established an artificial neural network model that could predict the radial force of esophageal stents based on the content of TPU, PCL and print parameter. We selected three optimal ratios for mechanical performance tests and evaluated the biomechanical effects of different ratios of stents on esophageal implantation, swallowing, and stent migration processes through finite element numerical simulation and in vitro simulation tests. The results showed that different ratios of polymer stents had different mechanical properties, affecting the effectiveness of stent expansion treatment and the possibility of postoperative complications of stent implantation.

KEYWORDS

Finite element method; 3D printing; polymer esophageal stent; artificial neural network

1 Introduction

Esophageal stricture is a common symptom of esophageal disease, mostly due to esophageal cancer, post-endoscopic dilatation, esophageal perforation, fistula, acid reflux, and chemical erosion [1–3]. Esophageal stenting is an effective palliative treatment for malignant esophageal and esophageal

fistulae to relieve dyspnea and dysphagia [4,5]. The types of stents widely used in esophageal stenting are self-expanding plastic stents (SEPS) and self-expanding metal stents (SEMS) [6,7]. Although metallic stents are widely used for clinical treatment because of their excellent compressibility and flexibility, such stents can cause complications such as inflammation, bleeding, and perforation [8]. To avoid such complications in patients with benign lesions, scholars have begun to develop polymeric esophageal stents that are better adapted to the individual patient using 3D printing technology [9,10]. This type of esophageal stent can be selected according to the patient's esophageal stricture site, length, diameter, morphology, and other factors, such as the appropriate stent type, size, and material, to achieve the best treatment results and reduce the probability of complications.

The mechanical properties of the stent and its structure have a very significant impact on the interaction between the stent and the esophageal wall. Therefore, it is necessary to conduct studies on the therapeutic purpose of stent implantation *in vivo*, the expected results, and the prevention of postoperative complications. However, in clinical practice, it is difficult to accurately predict the stent implantation plan and outcome. Therefore, it is necessary to use finite element software to simulate the mechanics of the stent and esophagus to study the effect of the stent implant on the human esophagus after the surgical implantation of the stent, which can assist practitioners to design individualized treatment protocols for patients.

Finite element analysis has been widely used in clinical medicine [11–13], as it saves a lot of time as well as economic costs, and the results obtained are very close to the real experimental results, regardless of the spatial constraints of the site [14,15]. Thus, the FE model analysis is an effective alternative method for interventional stent studies.

To address the issue of esophageal stent intervention, considering the expansion of the stent in the esophageal model, studies related to the analysis of the interaction and force changes with the esophagus during the release of the stent have received the attention of scholars. Peirlinck et al. developed a mechanical model of bioresorbable polymer braided wire stent-esophagus interaction [16]. Mozafari et al. applied the finite element method to quantitatively describe the effects of stent end shape, stent diameter, and friction coefficient on stent migration [17]. Ni et al. evaluated the influence of different end shapes of stents on the biomechanical interaction between stent and esophagus [18]. However, the current finite element simulation studies on stents mainly focus on braided stents, and less prevalent on 3D-printed polymeric esophageal stents. Compared to traditional means of stent manufacturing, 3D printing offers rapid manufacturing of personalized patient-specific medical devices, and implants with precise geometry [19,20].

BP neural network is a kind of multilayer perceptron based on error backpropagation algorithm, which can be used to solve nonlinear regression and classification problems, with learning ability and generalization ability [21,22]. By using the BP neural network to predict the material parameters of 3D printed esophageal stent, the optimal material performance and process parameters can be obtained quickly and accurately according to the historical data and influencing factors, which can improve the quality and efficiency of 3D printed esophageal stent [23]. Therefore, by applying the BP neural network models and finite element methods to 3D printing technology, the biomechanical properties and manufacturing parameters of stents can be rapidly simulated and optimized.

In this paper, we established a multi-objective artificial neural network model to predict the radial force of the esophageal stent and determine the optimal fabrication parameters of the esophageal stent. We selected three optimal ratios of the esophageal stent for finite element mechanical simulation and in vitro experiments to analyze the structural characteristics that affect the support strength and safety of the 3D printed polymer stent from the mechanical perspective. By numerically simulating the

release process, swallowing process and migration process of the polymer stent in a simple esophageal model, we found the relevant factors that affected the stent expansion effect. This can provide valuable references for physicians when using stent implantation therapy.

2 Materials and Methods

2.1 Fabrication of Esophageal Stent and Esophageal Model

The esophageal stent was 3D printed using the G5 screw extrusion 3D printer from Shenzhen Creality 3D Technology Co., Ltd. (Shenzhen, China). The total length of the stent is 61 mm, with a cylindrical segment of 45 mm in length and 20 mm in diameter in the middle; the two ends are bell-shaped with a length of 8 mm and a diameter of 28 mm, and there are 10 rings with a spacing of 5 mm in the middle part of the stent (Fig. 1) [24]. The stent is composed of thermoplastic polyurethane (TPU) and Poly-ε-caprolactone (PCL). We fabricated three different ratios of esophageal stents, 60TPU40PCL (60% content of TPU, 40% content of PCL), 70TPU30PCL (70% content of TPU, 30% content of PCL), and 80TPU20PCL (80% content of TPU, 20% content of PCL), which have different stiffness and rigidity. Information on the process and details of esophageal stent fabrication can be found in reference [24].

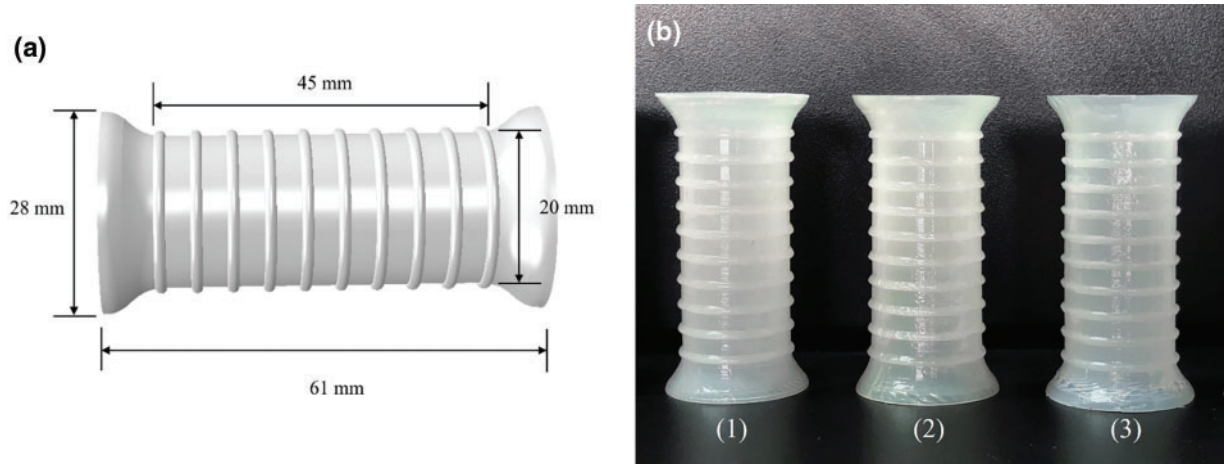

Figure 1: (a) Structural parameters of 3D printed esophageal stent. (b) 3D printing of TPU/PCL polymer stents with different ratios (from left to right are 1. 60TPU40PCL, 2. 70TPU30PCL, 3. 80TPU20PCL)

The esophageal model was fabricated using silicone with shore A hardness of 30 through the process of injection molding. To confirm the consistency between experiments and simulations, the dimensions of the esophageal model were the same as in the simulation model. Simplify the esophagus as a uniform cylinder with a length of 150 mm, an inner diameter of 18 mm, and a wall thickness of 3 mm.

2.2 Artificial Neural Network

2.2.1 Selection of Input Parameters

The objective of this work is to develop an artificial neural network model for predicting the mechanical properties of 3D printed polymer esophageal scaffolds. 4 input parameters were selected: (1) TPU content; (2) PCL content; (3) Printing temperature; (4) Filling density. The radial force of the

esophageal stent was predicted. The radial force of the esophageal stent determines the therapeutic effect after implantation. The radial force is too low to open the narrowed esophagus, and the radial force is too high, which will cause excessive pressure in the esophagus, leading to complications such as bleeding, so it is necessary to calculate the radial force of the esophageal stent according to the printing parameters and material parameters. We used the planar compression method to test the radial force of the esophageal stent [25]. Table 1 lists the values of the model training set and test set. Considering the requirement of BP neural network establishment, the number of specimens was therefore supplemented on the basis of the orthogonal test design scheme. 12 data sets are considered in the model, with 70% of the data as the training set and 30% of the data as the test set.

Table 1: Test scheme and results

No.	TPU content (%)	PCL content (%)	Printing temperature (°C)	Filling density (%)	Radial force (N)
1	80.00	20.00	210.00	100.00	5.80
2	80.00	20.00	220.00	80.00	5.20
3	80.00	20.00	210.00	90.00	5.50
4	70.00	30.00	210.00	90.00	9.90
5	70.00	30.00	200.00	80.00	9.50
6	70.00	30.00	210.00	100.00	10.30
7	60.00	40.00	210.00	80.00	12.20
8	60.00	40.00	220.00	90.00	12.70
9	60.00	40.00	210.00	100.00	13.10
10	60.00	40.00	200.00	100.00	12.80
11	70.00	30.00	220.00	100.00	10.20
12	80.00	20.00	200.00	90.00	5.40

2.2.2 Design of the BP Neural Network

Since the calculation for this experiment is relatively simple and the data is small, a common three-layer BP neural network structure with an input layer, a hidden layer and an output layer is chosen, as shown in Fig. 2. The accuracy of the network mainly depends on the number of nodes in the hidden layer, and the number of nodes in the hidden layer can be determined according to the following empirical equation:

$$l = \sqrt{n+m} + a, \tag{1}$$

where m is the number of output neurons, n is the number of input neurons, and a is the constant values ranging from 1 to 10. The number of neurons in the input layer (n) is 4, and the number of neurons in the output layer (m) is 1, which is the radial force of the stent. According to the empirical Eq. (1) and the experimental method, the number of neurons in the hidden layer (l) is finally determined as 11.

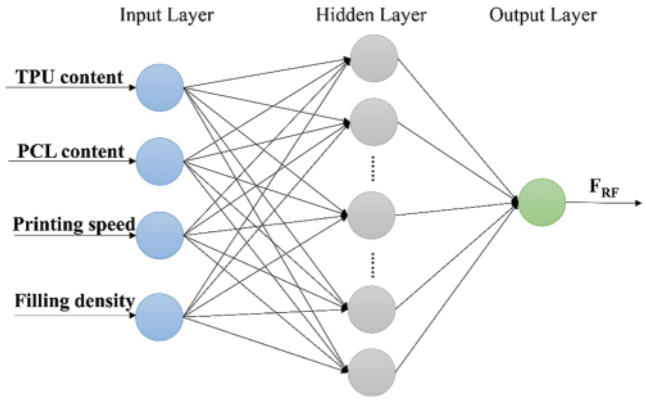

Figure 2: BP neural network structure diagram

The trainlm of the Levenberg-Marquardt (L-M) optimization algorithm is adopted as the training function. To ensure uniformity in the level of test input and output data, it is necessary to normalize all data by Eq. (2) so that the values converge between 0 and 1 [26]. Finally, the actual predicted output value could be obtained after inverse normalization of the output value by Eq. (3).

$$x_n = \frac{x - x_{\min}}{x_{\max} - x_{\min}}, \tag{2}$$

$$x_n = x_{\min} - x_n \cdot (x_{\max} - x_{\min}), \tag{3}$$

where x_n is the standardized data, x is the experimental data or the data after de-standardization; and $x_{\min}$ and $x_{\max}$ are the minimum and maximum values of the experiment, respectively [27]. The parameters of this BP neural network model are set as follows: trainlm of the Levenberg-Marquardt (L-M) optimization algorithm is chosen as the training function, the output layer neuron function uses purelin, the maximum training times is 1,000, the training target is 0.0001, and the learning rate is 0.01.

2.3 Finite Element Model of the Esophageal Stent and Simplified Esophagus

2.3.1 Hyperelastic Material Parameters and Modeling

The stent was made of TPU/PCL hyperelastic polymer, so the Mooney–Rivlin hyperelastic model is used for calculation. The hyperelastic constants of the Mooney–Rivlin model are obtained from the unidirectional tensile test, and the σ-ε curves are fitted and calculated by ABAQUS software to automatically generate the Mooney–Rivlin hyperelastic constants. The hyperelastic constants of TPU/PCL hyperelastic materials and esophagus are listed in Table 2 [17]. The strain energy density function of the Mooney–Rivlin model is:

$$W = c_{10}\left(\overline{I}_1 - 3\right) + c_{01}\left(\overline{I}_2 - 3\right) + c_{20}\left(\overline{I}_2 - 3\right)^2 + c_{11}\left(\overline{I}_1 - 3\right)\left(\overline{I}_2 - 3\right) + c_{02}\left(\overline{I}_2 - 3\right)^2 + \frac{1}{D_1}(J-1)^2, \tag{4}$$

where I_1 and I_2 are the strain invariants, W is the strain energy density function, and c_{10}, c_{01}, c_{11}, c_{20}, c_{02}, and D_1 are the hyperelastic constants. The simulated curves fitted by the Mooney–Rivlin model agree well with the experimental stress-strain curves (Fig. 3).

We assume that TPU/PCL polymer and esophageal tissue are completely incompressible materials and use C3D8R elements (8-node linear brick) for meshing, with 21,158 mesh elements and 29,700 mesh elements for the stent and esophageal models, respectively.

Table 2: Mooney–Rivlin parameters of composite materials and esophagus

	c_{10} (MPa)	c_{01} (MPa)	c_{11} (MPa)	c_{20} (MPa)	c_{02} (MPa)
80TPU/20PCL	−10.600	15.180	−0.271	3.089E-02	3.492
70TPU/30PCL	−13.638	19.388	−0.283	3.048E-02	4.363
60TPU/40TPU	−20.229	28.414	−0.419	4.496E-02	6.437
Esophagus	−0.027	0.048	0.812	−1.723	0.982

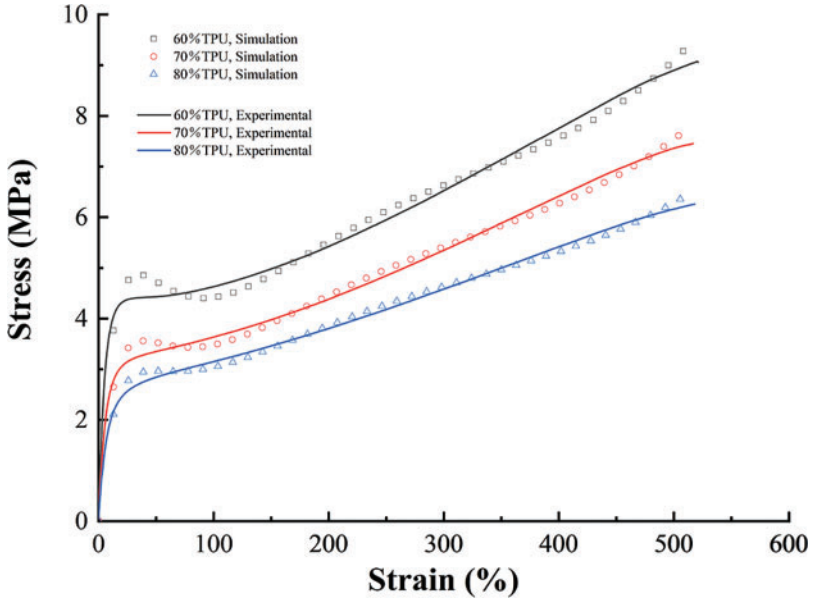

Figure 3: The experimental curves and their fitted counterparts (n = 5)

2.3.2 Boundary Condition Set

Taking the center point of the flared plane at one end of the stent as the coordinate origin, establish the cylindrical coordinate system with the axis of the cylindrical surface as the Z-axis and the T-axis direction as the radial direction of the stent. Create a shell to simulate the clamping process of the esophageal stent, and this shell should only be used for the clamping process of the esophageal stent, and will not interact with other parts of the model. The esophageal stent is pressed into the esophageal model until it reaches the preset position, remove the contact relationship between the clamping shell and the esophageal stent, release the compression state of the stent, activate the contact relationship between the stent and the esophageal wall, and make the esophageal stent self-expand to contact with the esophagus and reach mechanical equilibrium (Fig. 4). To ensure the convergence of the calculation and avoid the numerical instability and long simulation time involved in the simulation, the model of the stent is simplified by removing the circle of the cylindrical segment.

2.4 Radial Compression Test of Esophageal Stents

Fig. 5 shows our homemade delivery system and a schematic diagram of the stent when it is implanted into the delivery system. The system consists of a silicone hose with a size of 12 mm inner diameter and 14 mm outer diameter and a conveying head end. The homemade delivery system

is designed to simulate the clinical process of esophageal stent implantation. After implantation of the esophageal stent into the simple esophageal model, the esophageal stent is deformed by the compression of the esophageal model. Therefore, the percentage of shrinkage was measured by the compression rate ϕ. The compression rate of the esophageal stent is calculated by Eq. (5):

$$\phi = \left(1 - \frac{d}{D}\right) \times 100\%, \tag{5}$$

where D is the internal diameter at the flare of the esophageal stent before deformation, d is the internal diameter of the esophageal stent after deformation.

Figure 4: Simulate the process of releasing and unfolding the stent

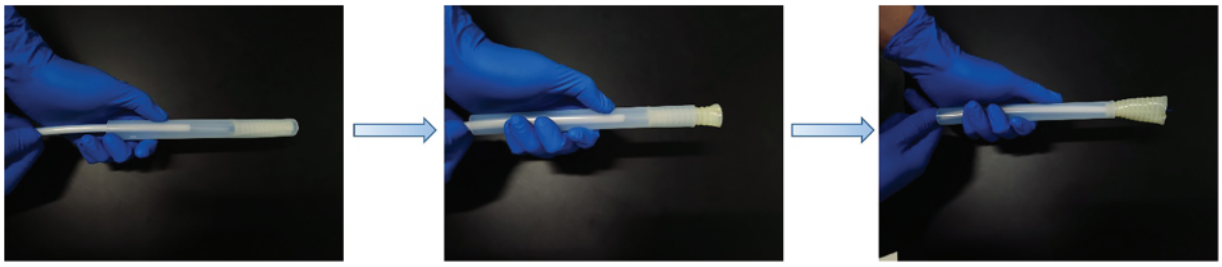

Figure 5: A homemade delivery system and conveying process

2.5 Anti-Migration Test in Simplified Esophageal Model

A simple esophagus model made of silicone was used for testing the anti-migration force of the stent (Fig. 6). Make a hole in the upper end of the esophageal stent and tie it to the universal testing machine with a rope. Fix the lower end of the esophageal model with the UTM-1422 universal testing machine, and fix the upper end with a rope on both sides of the universal testing machine. Then, set the universal testing machine to move uniformly upward at a rate of 50 mm/min, simulating the anti-migration force of the esophageal stent in the esophagus, and set the displacement distance to 50 mm [9].

3 Results and Discussion

3.1 Comparative Analysis of Prediction Models

Fig. 7a shows the trend of MSE change during the training of the BP neural network. It can be seen that the best training performance is 0.00024, at epoch 4. The performance of the training set in the BP neural network model is shown in Fig. 7b. It is clear that the fitted values of the BP neural network model are in good agreement with the experimental values with a correlation coefficient of 0.99682. By comparing and analyzing the experimental values and the predicted values of the BP neural network model in Table 3, we found that the maximum absolute error between them was no more than 8%, indicating that the BP neural network model had a good prediction effect on the radial force of the stent. Therefore, in the manufacturing process of esophageal stents, we can establish BP

neural network models for prediction based on the process effects obtained with different process parameters. For the subsequent mechanical property tests, esophageal stents with different ratios were selected, with a fixed printing temperature of 210°C and a filling density of 100%.

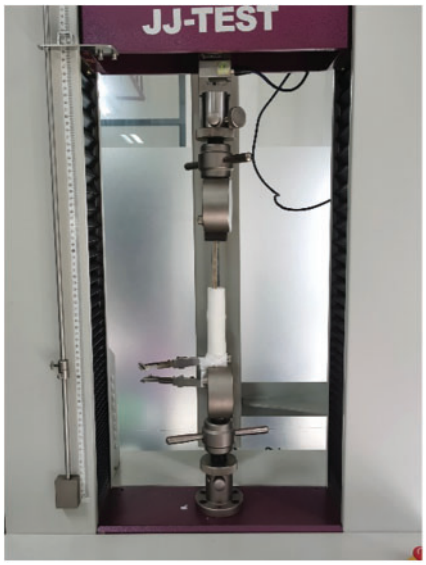

Figure 6: Anti-migration force test

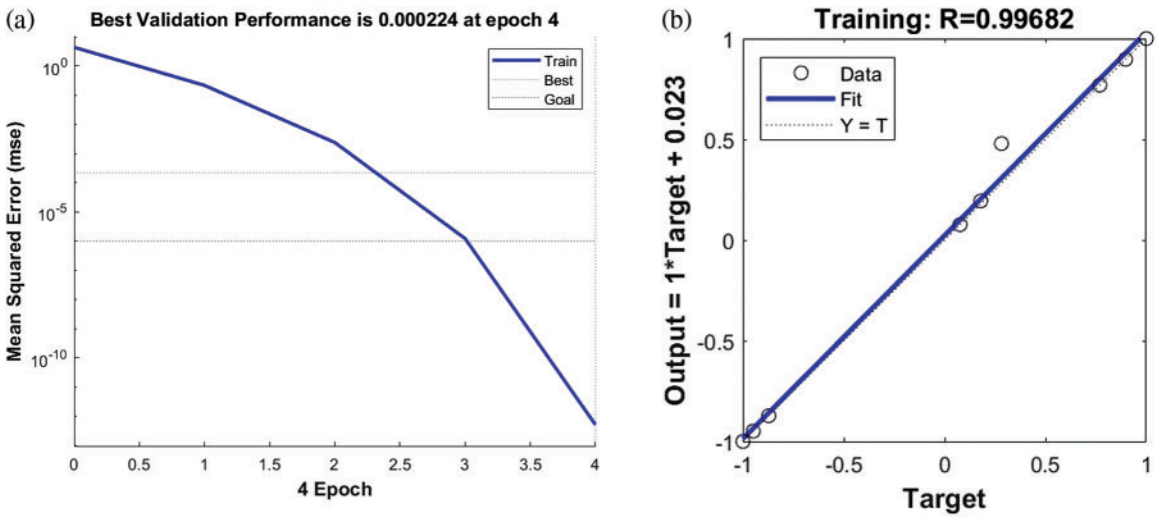

Figure 7: (a) Training mean squared error curve. (b) The curve fitting of training set

Table 3: Comparison of actual and testing values

No.	Actual (N)	Predicted (N)	Absolute (N)	Relative (%)
10	12.8	13.6	0.8	5.88
11	10.2	11.0	0.8	7.27
12	5.4	5.2	0.2	3.70

3.2 Interaction of Esophageal Stent Implantation into the Esophagus

The compression rates of different ratios of esophageal stents and the deformation and equivalent forces of the esophagus are listed in Table 4.

Table 4: Deformation and equivalent forces of the esophagus and stent in the coupled state (n = 3)

Sample designation	Maximum von Mises stress (kPa)	Outside diameter of the lumen at the flare after deformation (simulation) (mm)	Outside diameter of the lumen at the flare after deformation (test) (mm)
80TPU20PCL	144.0	31.75	31.17
70TPU30PCL	152.6	31.96	31.82
60TPU40PCL	169.8	32.15	32.11

Simulation results show that after the esophageal stent is implanted into the esophagus, the maximum elastic strain generated by the stent and the esophagus is mainly located in the flared section at both ends, while the elastic strain generated by the middle cylindrical section is relatively small. Comparing the mechanical performance of the three different stents during compression, the 60TPU40PCL caused the largest equivalent force on the esophagus at 161.7 kPa, the 70TPU30PCL stent was the second largest at 152.6 kPa, and the 80TPU20PCL was the smallest at 144 kPa. This is consistent with the results obtained by Yan et al. in their biomechanical finite element simulations of braided esophageal stents in terms of the trends of equivalent forces and strains generated during compression of the stent [28]. The mechanical environment of esophageal tissue can affect its performance. Experiencing mechanical signals outside the physiological range of the tissue (e.g., excessive stress after stent implantation) can negatively affect the normal physiological function of esophageal tissue. Saxena et al. noted that if the applied stress is significantly outside the physiological range, it may lead to the destruction of myogenic fibers, which can trigger pathological conditions [29]. Therefore, the appropriate stent type needs to be selected according to the pressure exerted by the stent on the esophageal wall.

Furthermore, we verify the validity of the simulation by in vitro tests. After implanting the esophageal stent into the esophageal model through the homemade delivery system, the deformation of the esophageal model was measured using vernier calipers (Fig. 8). It can be seen from Table 4 that the measurement of the deformation of the outer diameter of the esophagus is in good agreement with the simulation results. The difference between the test results and the simulation results does not exceed 10%.

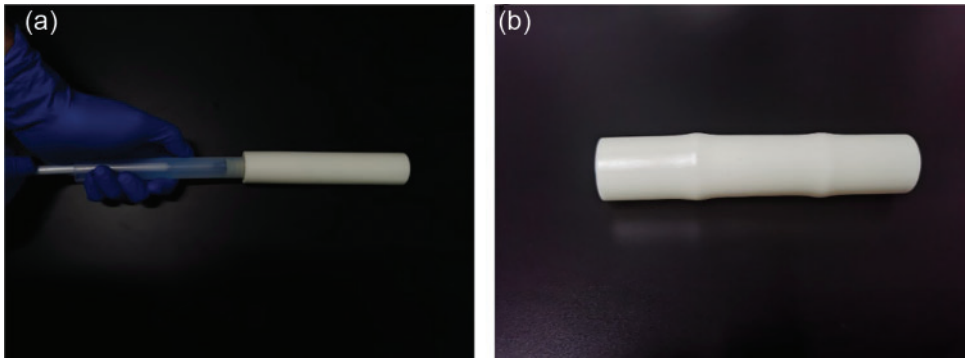

Figure 8: (a) Homemade delivery system for esophageal stent delivery. (b) Snapshot of the stent-implanted esophageal model

3.3 Numerical Simulation of Esophageal-Stent System Model under Swallowing Action

When the body chews and swallows food, the esophagus generates contractions and peristalsis waves to push the food forward. Esophageal contraction waves following swallowing can be viewed simply as triangular waves [30]. In biomedicine, esophageal peristalsis generates peristaltic wave loads of up to 9.8 kPa [31]. After implantation into the lumen of the esophagus, the stent is subjected to esophageal peristaltic waves and the stent is in a cyclic pulsatile load operating state. The peristaltic wave generated by the esophagus should be a moving fluctuating load, but the peristaltic wave that changes with time and spatial position cannot be simply realized in the process of finite element analysis. Therefore, in this paper, the moving peristaltic wave is simply treated so that the whole segment of the esophageal stent is subjected to a cyclic load with a peak value of 9.8 kPa [32]. Therefore, in simulating the radial compression ratio of the esophageal stent, the inner wall of the esophagus is made to generate a cycle of radial pressure to simulate the contraction deformation of the esophageal stent in the esophagus, and the peristaltic wave loading period is shown in Fig. 9. The deformation and stresses on the stent caused by the peristaltic wave are shown in Fig. 10 and Table 5.

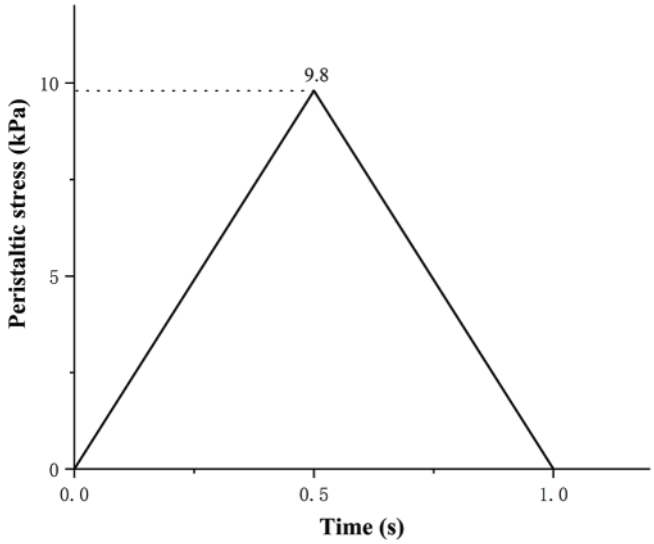

Figure 9: Peristaltic wave cycle

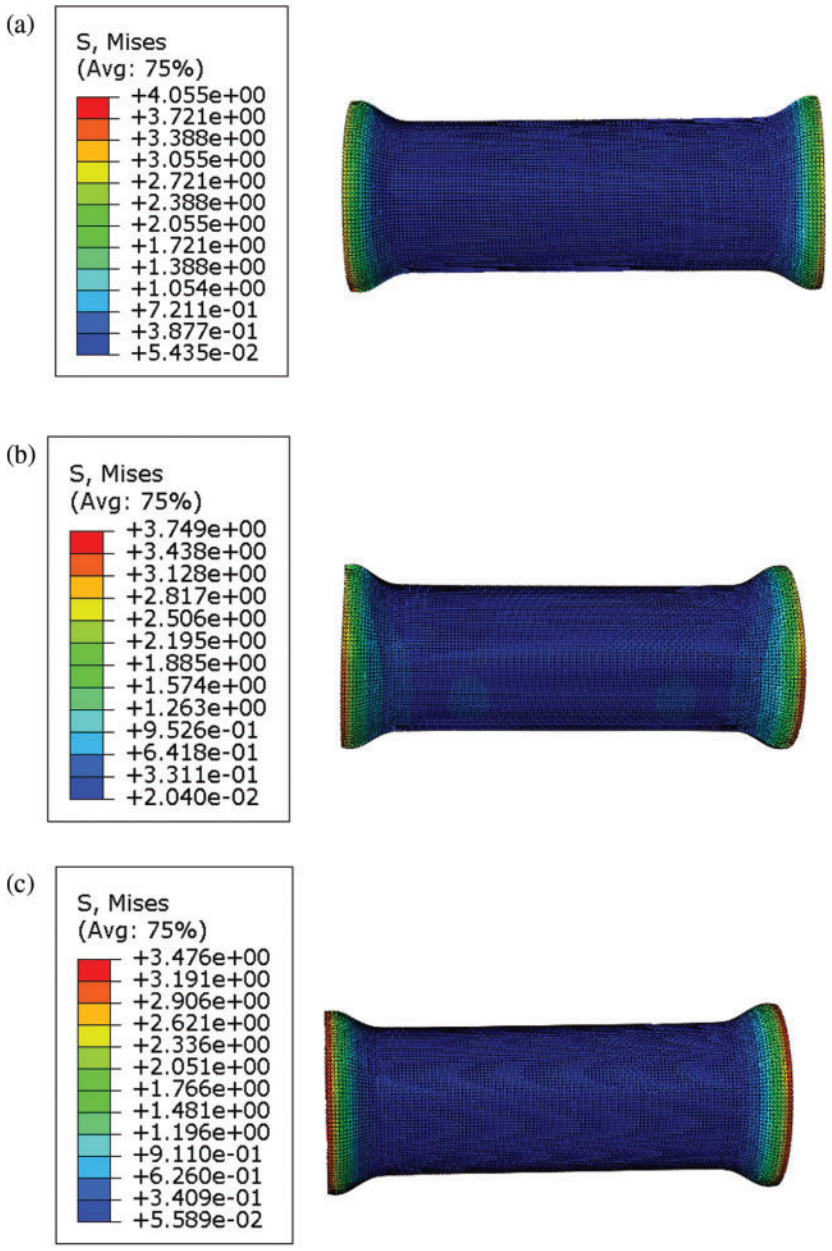

Figure 10: Maximum von Mises stress in different ratios of TPU/PCL stents under the action of peristaltic waves. (a) 60TPU40PCL. (b) 70TPU30PCL. (c) 80TPU20PCL

Table 5: Deformation and radial shrinkage of esophageal stents

Sample designation	Radial compression ratio ϕ (%)	Maximum von Mises stress (kPa)
80TPU20PCL	6.85	347.6
70TPU30PCL	6.07	374.8
60TPU40PCL	4.64	405.5

From the numerical calculations in the above table, it can be concluded that the compression rate of the esophageal stent is gradually decreasing as the PCL content of the stent increases. The 80TPU20PCL esophageal stent has the largest contraction rate of 6.85%, and the relevant literature indicates that patients with esophageal strictures usually feel difficulty swallowing only when the diameter of the esophagus is reduced by more than 25% [33]. Therefore, none of the above ratios of esophageal stents would cause excessive stent contraction due to the patient's swallowing pressure.

3.4 Anti-Migration Test Result

There exists a certain error between the finite element analysis results and the real condition, so the accuracy of the model needs to be verified by comparing the in vitro test with the finite element analysis results. Monitoring the contact force at the stent-esophagus during the pulling process. Fig. 11 presents the force-distance curves of the stent pulling process. The force-distance curves show a rising phase in the initial stage, and then become relatively stable. The esophageal stent of 60TPU40PCL had the highest anti-migration force of 10.4 N. With the increase in TPU content, the anti-migration force decreased. Greater anti-migration force decreases the probability of stent migration, thereby reducing the inherent complications associated with stents. However, excessive antimigration force may cause secondary damage to the mucosa due to stent removal [34,35]. The anti-migration test results of the esophageal stent system were similar to the finite element analysis.

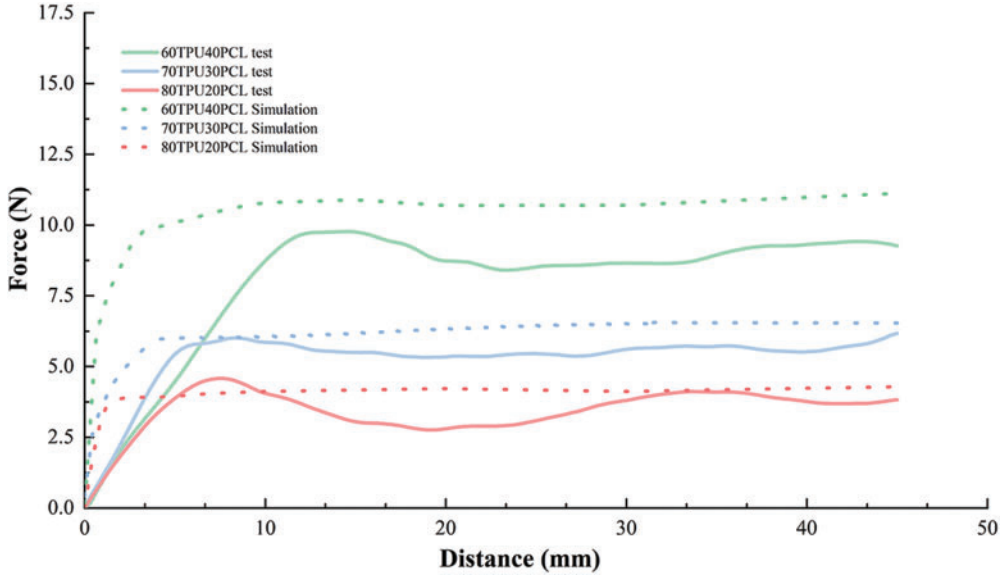

Figure 11: Force-distance curves for experimental and simulated migration processes

3.5 Numerical Simulation of Anti-Migration of the Esophageal Stent System

The esophageal stent was taken in displacement control mode, pulled out toward one end, and the stent-esophageal contact force was monitored during the pulling process (Fig. 12). We ensured that the initial and boundary conditions of the model were consistent with those of the subsequent experiments, to allow comparison of the results to verify the effectiveness of the simulation. The esophageal model was limited to movement in the R-axis direction, which ensured that the esophageal model could only be deformed in the radial direction and limited it to prevent rotational movement during stent

migration. We assumed that the friction factor between the outer surface of the stent and the inner surface of the esophageal wall was 0.1.

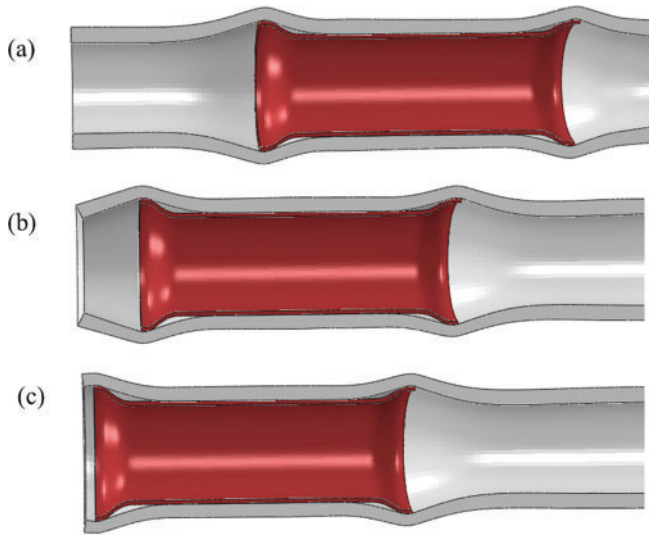

Figure 12: The esophageal stent pulling process

Fig. 13 depicts the distribution of stresses on the esophageal wall caused by different ratios of TPU/PCL polymer stents during pulling. It can be seen that the static stresses caused by the esophageal stent on the esophageal wall are on average 10–20% lower than the dynamic.

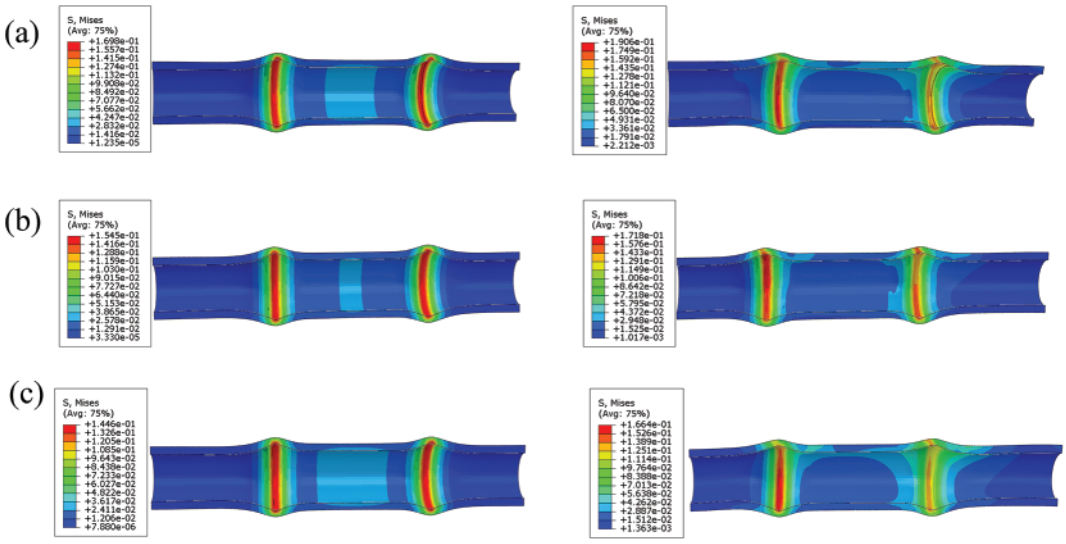

Figure 13: Stress distribution of TPU/PCL esophageal stents on the esophageal wall during static (left) and pulling (right) process. (a) 60TPU40PCL. (b) 70TPU30PCL. (c) 80TPU20PCL

As shown in Fig. 11, the dynamic process of stent migration was studied by pulling the stent through the esophagus. By comparing the force and distance curves of the experimental and simulated processes, it can be found that the peak anti-migration force of the simulated and experimental results

of the esophageal stent are very close, and the trend of the anti-migration force of different ratios of TPU/PCL polymer stents is also consistent with the experimental results. In the force-distance curve simulated by FEA, the peak force is reached at a distance of approximately 3 mm, while the peak force measured by the test is reached at a distance of approximately 8 mm. This error may be due to some difference between the boundary condition setting of the simulation and the real test, which does not affect our analysis of the anti-migration capacity of the stent.

3.6 Discussion

It has been documented [18] that the commercial woven metal esophageal stent implantation resulted in a maximum equivalent force of 0.649 MPa on the healthy area, while the TPU/PCL polymer esophageal stent caused a maximum equivalent force of 0.170 MPa on the esophagus, which proved that the polymer esophageal stent could alleviate the patient's discomfort and reduce the probability of complications after stent implantation.

To verify the mechanical behavior of the stent during dynamic migration motion, we analyzed the dynamic motion model of the esophageal stent and the stationary model. The results show that the esophageal stent causes greater equivalent forces on the esophageal wall during dynamic migration. This is due to increased local stress caused by stretching, pressing, and rubbing motions between the esophageal stent and the esophagus.

The mechanical properties of esophageal stents depend mainly on the material, structure, and process of the esophageal stent, and the most variable of them is the structure of the stent. An excellent design of stent structure can significantly improve the comfort of patients after stent implantation, and a too sharp stent structure can increase the probability of complications [36]. Therefore, finite element simulation plays a crucial role in the design of esophageal stents, which can provide a reference for optimizing the performance parameters of the stent fabrication process.

Although this paper makes several unique contributions to the existing literature, it does have limitations. The stent is implanted into the human body, and the fluctuation of the swallowing process is generated inside the human body, and under the effect of this long-term high-frequency pulsatile pressure, the stent fatigue problem becomes an important influence on the service time of the stent. In future research, the fatigue problem of stents should be further explored.

In this paper, the finite element model of the esophagus is simplified to ensure that the model for in vitro testing is easier to fabricate. The modeling of the esophageal tumor part was not considered in our study because it was found in the clinical treatment that the material properties of the tumors differed significantly from patient to patient [37], and the differences in material and structure of these tumors could cause some differences in the calculation results. Although the esophagus is a simple tubular organ, it mainly consists of the inner mucosa-submucosa layer and two outer muscle layers to form tissue offering structural as well as functional characteristics [38]. Therefore, alternative models of the esophagus need to be made in the future according to the biomechanical specifications of the esophageal tissue. In the next step, we will consider inverse modelling of the real esophagus model based on the CT scan data of the patient, which will help to further personalize patient's esophageal stents [39,40].

4 Conclusions

In this paper, an artificial neural network model was developed to predict the radial force of the esophageal stent based on the input variables which include TPU content, PCL content, printing temperature, filling density. The model showed a high accuracy with a small relative error

and a correlation coefficient of 0.99962 compared to the experimental values. Furthermore, finite element analysis was performed to simulate the implantation release process, esophageal swallowing contraction process and dynamic migration process of 3D printed polymer stents with different ratios. The results demonstrated the necessity and feasibility of using the esophageal model to study the biomechanics of stent implantation. The stent exhibited good radial properties and maintained its normal shape without significant deformation under swallowing pressure. The simulation results were consistent with the data from the migration resistance test and radial shrinkage test of the stent. Finite element simulation can provide a realistic representation of the biomechanical environment and the therapeutic effect of stent implantation, as well as scientific guidance for stent design and clinical selection.

Acknowledgement: Thanks to the help of the editor and reviewers for their constructive comments and suggestions, which have improved the logical organization and content quality of this paper have been improved.

Funding Statement: This work was financially supported by Nanning Technology and Innovation Special Program (20204122) and Research Grant for 100 Talents of Guangxi Plan.

Author Contributions: Conceptualization, P.Y. and B.Z.; methodology, P.Y., B.Z. and G.L.W.; validation, G.L.W., P.Y. and B.Z.; formal analysis, S.H.H., T.T.L., Z.N.Y., G.H.W. and Y.S.W.; investigation, S.H.H., T.T.L., Z.N.Y., G.H.W., Y.S.W., Q.L.Z. and J.F.; data curation, S.H.H., T.T.L., Z.N.Y., G.H.W., Y.S.W., Q.L.Z. and J.F.; writing—original draft preparation, G.L.W., S.H.H., T.T.L., Z.N.Y., G.H.W. and Y.S.W.; writing—review and editing, P.Y., B.Z.; supervision, Q.L.Z. and J.F. All authors have read and agreed to the published version of the manuscript.

Availability of Data and Materials: The datasets used or analyzed in this study are available upon request from the corresponding author.

Conflicts of Interest: The authors declare that they have no conflicts of interest to report regarding the present study.

References

1. Qi, L., He, W., Yang, J., Gao, Y., Chen, J. (2018). Endoscopic balloon dilation and submucosal injection of triamcinolone acetonide in the treatment of esophageal stricture: A single-center retrospective study. *Experimental and Therapeutic Medicine, 16(6),* 5248–5252.
2. Cao, F., Chen, G., Su, W., Zhang, Z., Fu, Q. et al. (2022). Endoscopic ultrasound-guided fine needle aspiration for smooth benign appearing malignant esophageal stricture: A cross-sectional study. *Journal of Thoracic Disease, 14(6),* 2112–2121.
3. Siersema, P. D. (2009). Stenting for benign esophageal strictures. *Endoscopy, 41(4),* 363–373.
4. Sharma, P., Kozarek, R., Gastroenterology, P. P. C. O. (2010). Role of esophageal stents in benign and malignant diseases. *American Journal of Gastroenterology, 105(2),* 258–273. https://doi.org/10.1038/ajg.2009.684
5. Park, J., Jeong, S., Lee, D. H. (2015). Recent advances in gastrointestinal stent development. *Clinical Endoscopy, 48(3),* 209–215.
6. Kang, Y. (2019). A review of self-expanding esophageal stents for the palliation therapy of inoperable esophageal malignancies. *Biomed Research International, 2019(8),* 1–11. https://doi.org/10.1155/2019/9265017

7. Didden, P., Spaander, M., Bruno, M. J. (2013). Esophageal stents in malignant and benign disorders. *Current Gastroenterology Reports, 15(4),* 1–9.
8. Dubecz, A., Watson, T. J., Raymond, D. P., Jones, C. E., Matousek, A. et al. (2011). Esophageal stenting for malignant and benign disease: 133 cases on a thoracic surgical service. *The Annals of Thoracic Surgery, 92(6),* 2028–2033. https://doi.org/10.1016/j.athoracsur.2011.08.033
9. Lin, M., Firoozi, N., Tsai, C., Wallace, M. B., Kang, Y. (2019). 3D-printed flexible polymer stents for potential applications in inoperable esophageal malignancies. *Acta Biomaterialia, 83(4),* 119–129. https://doi.org/10.1016/j.actbio.2018.10.035
10. Fouladian, P., Kohlhagen, J., Arafat, M., Afinjuomo, O., Workman, N. et al. (2020). Three-dimensional printed 5-fluorouracil eluting polyurethane stents for the treatment of oesophageal cancers. *Biomaterials Science, 8(23),* 6625–6636. https://doi.org/10.1039/D0BM01355B
11. Mei, Y., Hurtado, D. E., Pant, S., Aggarwal, A. (2018). On improving the numerical convergence of highly nonlinear elasticity problems. *Computer Methods in Applied Mechanics and Engineering, 337,* 110–127. https://doi.org/10.1016/j.cma.2018.03.033
12. Deng, J., Guo, X., Mei, Y., Avril, S. (2023). Fenics implementation of the virtual fields method (VFM) for nonhomogeneous hyperelastic identification. *Advances in Engineering Software, 175,* 103343. https://doi.org/10.1016/j.advengsoft.2022.103343
13. Mei, Y., Liu, J., Guo, X., Zimmerman, B., Nguyen, T. D. et al. (2021). General finite-element framework of the virtual fields method in nonlinear elasticity. *Journal of Elasticity, 145(1),* 265–294. https://doi.org/10.1007/s10659-021-09842-8
14. Ma, T., Dong, Z. H., Wang, S., Meng, Z. Y., Chen, Y. Y. et al. (2018). Computational investigation of interaction between stent graft and aorta in retrograde type A dissection after thoracic endovascular aortic repair for type B aortic dissection. *Journal of Vascular Surgery, 68(6),* 14S–21S.
15. Wu, W., Wang, W., Yang, D., Qi, M. (2007). Stent expansion in curved vessel and their interactions: A finite element analysis. *Journal of Biomechanics, 40(11),* 2580–2585. https://doi.org/10.1016/j.jbiomech.2006.11.009
16. Peirlinck, M., Debusschere, N., Iannaccone, F., Siersema, P. D., Verhegghe, B. et al. (2018). An *in silico* biomechanical analysis of the stent-esophagus interaction. *Biomechanics and Modeling in Mechanobiology, 17(1),* 111–131. https://doi.org/10.1007/s10237-017-0948-9
17. Mozafari, H., Dong, P., Zhao, S., Bi, Y., Han, X. et al. (2018). Migration resistance of esophageal stents: The role of stent design. *Computers in Biology and Medicine, 100(7),* 43–49. https://doi.org/10.1016/j.compbiomed.2018.06.031
18. Ni, X., Zhang, Y., Zhao, H., Pan, C. (2018). Numerical research on the biomechanical behaviour of braided stents with different end shapes and stent-oesophagus interaction. *International Journal for Numerical Methods in Biomedical Engineering, 34(6),* e2971. https://doi.org/10.1002/cnm.2971
19. Zhu, Y., Joralmon, D., Shan, W., Chen, Y., Rong, J. et al. (2021). 3D printing biomimetic materials and structures for biomedical applications. *Bio-Design and Manufacturing, 4(2),* 405–428. https://doi.org/10.1007/s42242-020-00117-0
20. Eshkalak, S. K., Ghomi, E. R., Dai, Y., Choudhury, D., Ramakrishna, S. (2020). The role of three-dimensional printing in healthcare and medicine. *Materials & Design, 194,* 108940. https://doi.org/10.1016/j.matdes.2020.108940
21. Liu, Y., Zhang, M. (2018). *Neural network methods for natural language processing*, pp. 193–195. Cambridge, USA: MIT Press. https:/doi.org/10.1162/COLI_r_00312
22. Hu, C., Zhao, F. (2010). Improved methods of BP neural network algorithm and its limitation. *2010 International Forum on Information Technology and Applications*, pp. 11–14. Kunming, China, IEEE.
23. Mahmood, M. A., Visan, A. I., Ristoscu, C., Mihailescu, I. N. (2021). Artificial neural network algorithms for 3D printing. *Materials, 14(1),* 163. https://doi.org/10.3390/ma14010163

24. Yu, P., Huang, S., Yang, Z., Liu, T., Qilin, Z. et al. (2023). Biomechanical properties of a customizable TPU/PCL blended esophageal stent fabricated by 3D printing. *Materials Today Communications, 34,* 105196. https://doi.org/10.1016/j.mtcomm.2022.105196
25. Liu, Q., Lei, L., Zeng, P., Zhao, Y. (2010). Numerical and experimental study of radial support capacity of intravascular stent. *Zhongguo Yi Liao Qi Xie Za Zhi = Chinese Journal of Medical Instrumentation, 34(3),* 175–179.
26. Deng, L., Feng, B., Zhang, Y. (2018). An optimization method for multi-objective and multi-factor designing of a ceramic slurry: Combining orthogonal experimental design with artificial neural networks. *Ceramics International, 44(13),* 15918–15923. https://doi.org/10.1016/j.ceramint.2018.06.010
27. Li, Y., Ding, F., Tian, W. (2022). Optimization of 3D printing parameters on deformation by BP neural network algorithm. *Metals, 12(10),* 1559. https://doi.org/10.3390/met12101559
28. Yan, W., Yu, H., Ding, B., Zheng, Z., Yan, H. et al. (2022). Biomechanical study of new biodegradable esophageal stent. *Zhongguo Yi Liao Qi Xie Za Zhi = Chinese Journal of Medical Instrumentation, 46(2),* 126–131. https://doi.org/10.3969/j.issn.1671-7104.2022.02.002
29. Saxena, A. K., Biro, E., Sommer, G., Holzapfel, G. A. (2021). Esophagus stretch tests: Biomechanics for tissue engineering and possible implications on the outcome of esophageal atresia repairs performed under excessive tension. *Esophagus, 18(2),* 346–352. https://doi.org/10.1007/s10388-020-00769-y
30. Herbella, F. A., Armijo, P. R., Patti, M. G. (2016). A pictorial presentation of 3.0 Chicago classification for esophageal motility disorders. *Einstein-Sao Paulo, 14,* 439–442.
31. Conklin, J. L. (2013). Evaluation of esophageal motor function with high-resolution manometry. *Journal of Neurogastroenterology and Motility, 19(3),* 281–294.
32. Ni, X., Bo, C., Wang, Y., Ni, Z. (2009). Research on numerical simulation and structural fatigue life for esophagus stent. *China Mechanical Engineering, 20(23),* 2856–2860 (In Chinese).
33. Yang, C., Lin, H., Hsieh, T., Chang, W. (2015). Palliative enteral feeding for patients with malignant esophageal obstruction: A retrospective study. *BMC Palliative Care, 14(1),* 1–8.
34. Garbey, M., Salmon, R., Fikfak, V., Clerc, C. O. (2016). Esophageal stent migration: Testing few hypothesis with a simplified mathematical model. *Computers in Biology and Medicine, 79(2),* 259–265. https://doi.org/10.1016/j.compbiomed.2016.10.024
35. Ji, J., Lee, B., Kim, H., Cho, Y., Choi, H. et al. (2011). Antimigration property of a newly designed covered metal stent for esophageal stricture: An in vivo animal study. *Gastrointestinal Endoscopy, 74(1),* 148–153.
36. Shin, J. H., Song, H., Kim, J. H., Kim, S., Lee, G. H. et al. (2005). Comparison of temporary and permanent stent placement with concurrent radiation therapy in patients with esophageal carcinoma. *Journal of Vascular and Interventional Radiology, 16(1),* 67–74.
37. Nasir, B. S., Tahiri, M., Kazakov, J., Thiffault, V., Ferraro, P. et al. (2016). Palliation of concomitant tracheobronchial and esophageal disease using a combined airway and esophageal approach. *Annals of Thoracic Surgery, 102(2),* 400–406. https://doi.org/10.1016/j.athoracsur.2016.03.021
38. Sommer, G., Schriefl, A., Zeindlinger, G., Katzensteiner, A., Ainödhofer, H. et al. (2013). Multiaxial mechanical response and constitutive modeling of esophageal tissues: Impact on esophageal tissue engineering. *Acta Biomaterialia, 9(12),* 9379–9391. https://doi.org/10.1016/j.actbio.2013.07.041
39. Wang, B., Yang, L., Cheng, J., Wang, J., Mei, Y. (2023). *In-vivo* high-speed biomechanical imaging of the cornea using corvis ST and digital image correlation. *Computers in Biology and Medicine, 153,* 106540. https://doi.org/10.1016/j.compbiomed.2023.106540
40. Mei, Y., Du, Z., Zhao, D., Zhang, W., Liu, C. et al. (2021). Moving morphable inclusion approach: An explicit framework to solve inverse problem in elasticity. *Journal of Applied Mechanics, 88(4),* 041001. https://doi.org/10.1115/1.4049142